

# P2P-NET: Bidirectional Point Displacement Net for Shape Transform

KANGXUE YIN, Simon Fraser University

HUI HUANG, Shenzhen University

DANIEL COHEN-OR, Tel Aviv University

HAO ZHANG, Simon Fraser University

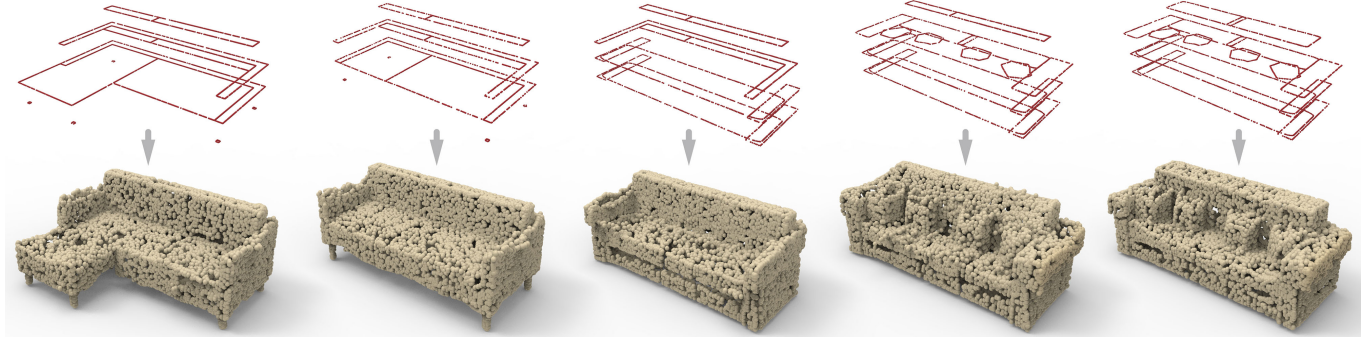


Fig. 1. We develop a general-purpose deep neural network which learns geometric transformations between point sets, e.g., from cross-sectional profiles to 3D shapes, as shown. User can edit the profiles to create an interpolating sequence (top) and our network transforms all of them into point-based 3D shapes.

We introduce P2P-NET, a *general-purpose* deep neural network which learns geometric transformations between point-based shape representations from two domains, e.g., meso-skeletons and surfaces, partial and complete scans, etc. The architecture of the P2P-NET is that of a *bi-directional point displacement* network, which transforms a source point set to a target point set with the same cardinality, and vice versa, by applying *point-wise* displacement vectors learned from data. P2P-NET is trained on *paired* shapes from the source and target domains, but *without* relying on point-to-point correspondences between the source and target point sets. The training loss combines two uni-directional geometric losses, each enforcing a *shape-wise* similarity between the predicted and the target point sets, and a cross-regularization term to encourage consistency between displacement vectors going in opposite directions. We develop and present several different applications enabled by our general-purpose bidirectional P2P-NET to highlight the effectiveness, versatility, and potential of our network in solving a variety of point-based shape transformation problems.

CCS Concepts: • **Computing methodologies** → **Computer graphics**; **Shape analysis**;

Additional Key Words and Phrases: Point cloud processing, deep neural network, point-wise displacement, point set transform

## 1 INTRODUCTION

Point primitives and point-based processing have drawn considerable interests from the computer graphics community for many

years [Gross and Pfister 2007]. As a fundamental shape representation, point sets are more compact than voxels and more flexible than polygon meshes, and they are immediately available as the default output from most 3D shape acquisition devices. Recently, deep neural networks have been designed to learn global and multi-scale point set features for shape classification and segmentation [Qi et al. 2017a,b], as well as geometry (e.g., normal or curvature) estimation [Guerrero et al. 2017]. Image-driven generative models have also been trained to reconstruct point-based 3D object representations from single or multi-view images [Fan et al. 2017; Lin et al. 2018; Lun et al. 2017].

In this paper, we are interested in exploring how deep neural networks can benefit a new class of problems in point-based graphics: *geometric transformations* between shapes represented by point sets. Such shape transforms span a wide spectrum of applications. Some examples include transforms between shape skeletons and surfaces, incomplete and completed object scans, 2D contours and 3D shapes, simplified and detailed surfaces, etc. Our goal is to develop a *general-purpose* neural network capable of learning geometric transformations between point sets from two domains. In computer vision, there have been a great deal of recent interests in solving a similar problem, but for images, namely, designing general-purpose, end-to-end image-to-image translation networks [Isola et al. 2017; Liu et al. 2017; Yi et al. 2017; Zhu et al. 2017].

Most successes on generic image translation have been achieved for tasks leading to “stylistic” changes in images without geometrically

This is the arXiv version of the work. It is posted here for your personal use. Not for redistribution.

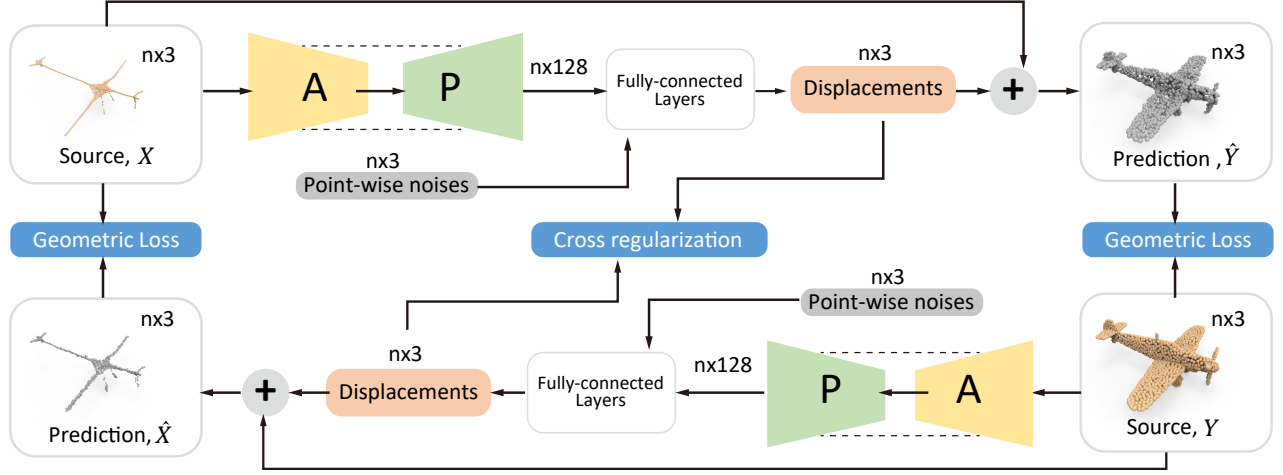


Fig. 2. Network architecture of our bidirectional P2P-NET.

transforming the image content. Such tasks include changing between night and day images, artistic styles, material properties, etc. Under this setting, some recent works such as CycleGAN [Zhu et al. 2017] and DualGAN [Yi et al. 2017] can train their translators *without* paired images, but they both rely on loss functions that measure pixel-to-pixel differences. Thus, while the images are not paired, the pixels are. When geometric changes are involved in the translation, these methods have all encountered significant obstacles.

In our current pursuit, the distinction, as well as the key novelty, of the problem is that transforming shape geometry is the goal. Furthermore, while pairing pixels is trivial when the image contents do not deform, pairing points as two point-based shapes are geometrically deformed is far from straightforward in general. For example, consider the task of transforming from a cross-sectional profile representation to a 3D shape (see Figure 1). Even if the two point sets are sampled from the same shape, there is no clear point-to-point correspondence between them. In our first attempt to develop a general-purpose transformation network for point sets, and in contrast to CycleGAN and DualGAN, we rely on paired shapes in training, but do not require paired points.

Specifically, we design a *point-to-point displacement* network, coined *P2P-NET*, which transforms an input point set to an output set with the same cardinality by applying *point-wise* displacement vectors learned from data. The P2P-NET is trained under a weakly-supervised setting, where paired point sets which share some commonality are provided, but not their point-wise mapping. In most of the applications considered, the commonality is that the two point sets were sampled from the same shape. However, in many applications, there is no clear point-to-point correspondence between the two point sets or the two sets could contain point samples acquired under different view settings or at different time instants. Not requiring point-wise correspondences can significantly expand our capacity to collect training data for P2P-NET.

Given two domains of point set data,  $\mathcal{X}$  and  $\mathcal{Y}$ , we introduce a *bidirectional* architecture to learn the two transformations  $\mathcal{X}$ -to- $\mathcal{Y}$  and  $\mathcal{Y}$ -to- $\mathcal{X}$ , simultaneously, as shown in Figure 2. Given a source point set  $X$ , the (bidirectional) P2P-NET learns to predict a set of displacement vectors  $I_X$  that are applied to  $X$  to obtain the predicted point set  $\hat{Y} = X + I_X$ . One objective of training the P2P-NET, defined by a *geometric loss*, is to make the predictions  $\hat{Y}$  as close as possible to the target *shape* represented by the point set  $Y$ . At the same time and along the opposite direction, the network also learns to predict displacements vectors  $I_Y$ , such that  $Y + I_Y$  is as close as possible to  $X$ , shape-wise. In addition, we define a *cross regularization* loss which couples and *mutually enhances* the two directional sub-networks by encouraging *parallelism* between the two sets of displacement vectors  $I_X$  and  $I_Y$ . Our bidirectional P2P-NET is trained with a combined loss consisting of two (directional) geometry terms and one cross regularization term. None of the loss terms requires a point-wise correspondence between  $X$  and  $Y$ .

Along each direction of the P2P-NET, the network takes a set of 3D points as input and first learns a multi-scale feature per point through set abstraction and feature propagation layers of PointNet++ [Qi et al. 2017b]. The learned features are then concatenated, point-wise, with a set of independent Gaussian noise vectors, and fed to a set of fully connected layers that finally produce a set of 3D displacement vectors, one per input point. The injection of per-point noise into the network provides added freedom for point displacements, effectively neutralizing potential local overfitting while improving smoothness of the predicted point set.

Note that P2P-NET learns point set transforms *implicitly*. It cannot learn how to transform each point in the source to its corresponding point in the target, since such point-to-point correspondences are not provided by training data. Instead, P2P-NET learns a mapping from point features (encoded as in PointNet++) to displacement vectors, which are applied to the source shape.

The main contributions of our work include:

- First general-purpose deep neural network designed to learn transformations between point-based shape representations.
- Bidirectionality of the network with a novel cross regularization loss to mutually enhance two directional transforms.
- Training losses defined without point-to-point correspondence, allowing the network to be trained under weak supervision.

We demonstrate how noise augmentation, cross regularization, and bidirectionality improve the performance of our P2P-NET as it carries out its learning tasks. We develop and present several different applications enabled by our general-purpose bidirectional P2P-NET to highlight the effectiveness, versatility, and potential of our network in solving a variety of point-based shape transformation problems. These include transforms between skeletons and shapes, between skeletons and scans, between partial and complete scans, and finally between cross-sectional profiles and 3D shapes.

## 2 RELATED WORK

The literature on point-based graphics and the application of deep neural networks to solve graphics problems is vast. In this section, we only cover the most relevant works to P2P-NET.

**Point processing.** Point cloud, as a 3D shape representation, has shown its advantages and applications in geometry modeling [Pauly et al. 2003], rendering [Alexa et al. 2003], and computer animation [Müller et al. 2004]. With the emergence of affordable 3D acquisition devices, point cloud data is widely captured, accumulated, and processed by many useful techniques, e.g., in point cloud filtering [Mitra and Nguyen 2003], resampling [Huang et al. 2013b], and surface reconstruction [Berger et al. 2017; Carr et al. 2001; Kazhdan and Hoppe 2013], to name just a few.

**Point set displacement.** Several past works took a displacement-based approach to process point sets. One such example is point set skeletonization, where point samples gradually coverge from a shape’s surface to a skeletal structure. The main challenge lies in how to deal with missing data over the latent surface, e.g., when the point scan was acquired from a single view. Tagliasacchi et al. [2009] propose a generalized rotational symmetry axis (ROSA) to extract curve skeletons from incomplete point clouds. Cao et al. [2010] apply a Laplacian-based contraction to extract curve skeletons. Huang et al. [2013a] introduce  $L_1$ -medial skeletons by adapting  $L_1$ -medians locally to an incomplete point set representing a 3D shape. Our P2P-NET leads to a data-driven approach to point cloud skeletonization and the bidirectional architecture also trains the network to perform the novel task of *skeleton-to-shape* transform.

Another example is surface completion by evolving point samples to gradually fill missing data over the latent surface. Representative methods include point cloud consolidation via LOP [Lipman et al. 2007] and WLOP [Huang et al. 2009; Preiner et al. 2014]. A more recent work that bridges point cloud skeletonization and consolidation [Wu et al. 2015a] spreads point samples regularly to cover gaps over surface regions via a joint optimization of surface and structure samples. Point cloud resampling can also be applied for edge

enhancements [Huang et al. 2013c]. P2P-NET offers a data-driven approach to surface completion, via point displacements, which offers an alternative to other learning-based surface completion techniques such as the recent work by Dai et al. [2017].

**Neural networks for point processing.** Neural networks excel in learning global features. A key development in connecting point sets to neural networks is PointNet [Qi et al. 2017a], which directly consumes unorganized point samples as input. This is followed by PointNet++ [Qi et al. 2017b], which enables hierarchical learning on point sets. In both cases, the input point set goes through point-wise or patch-wise feature transform followed by feature aggregation, either globally or locally, so as to serve the tasks of shape classification and segmentation (i.e., patch classification). Another multi-scale variant of PointNet, by Guerrero et al. [2017], is adapted for estimating local shape properties such as normals and curvatures. Sung et al. [2017] demonstrate the usefulness of PointNets for component suggestion in part-based shape assembly.

Our P2P-NET is designed to solve a different class of problems, namely, point displacement based shape transforms. While P2P-NET does employ the set abstraction and feature propagation layers of PointNet++ [Qi et al. 2017b] for feature learning, it combines the learned features with noise and trains a bidirectional network, with a novel loss term combining shape approximation and cross regularization, to obtain point displacement vectors.

There have been several recent attempts at developing deep generative networks for point-based shapes. Fan et al. [2017] design and train a neural network as a conditional sampler, which is capable of predicting multiple plausible 3D point clouds from a single input image. Multiple point clouds from different views have also been constructed as intermediate shape representations for the purpose of generating 3D shapes from 2D images and/or sketches [Lin et al. 2018; Lun et al. 2017]. Gadelha et al. [2017] synthesize point-based 3D shapes in the space of shape coefficients using a generative adversarial network (GAN). They build a KD-tree to spatially partition the points and then conduct PCA analysis to derive a linear shape basis and optimize the point ordering.

To the best of our knowledge, P2P-NET is the first deep neural network designed to learn geometric transformations between point-based shape representations.

**Learning transformations.** Several classical vision problems need to account for spatial transformations in images, e.g., recognizing objects undergoing deformations [Jaderberg et al. 2015] and synthesizing images under novel views [Zhou et al. 2016], just to name a few. Both works are representative of applying deep neural networks for their respective tasks. There have been considerable less effort on learning geometric transforms for 3D shapes. Recent attempts have been made to learn to transfer surface details [Berkiten et al. 2017], decorative styles [Hu et al. 2017], and to predict piecewise rigid transformations of 3D objects [Byravan and Fox 2016]. In contrast, our work aims to develop a *general-purpose* neural network for learning transformations between point-based 3D shapes.

**Paired vs. unpaired training data.** Analogous to our shape transform problem is general-purpose image-to-image translation [Isola et al. 2017; Liu et al. 2017; Yi et al. 2017; Zhu et al. 2017], where point displacements can be regarded as analogous to pixel-to-pixel transforms. An important feature of some of these recent works [Liu et al. 2017; Yi et al. 2017; Zhu et al. 2017] is that the training does not require paired images. On the other hand, these works, which rely on deep generative neural networks such as GANs, have only shown success in color and texture transforms, e.g., for altering painting styles or material properties of imaged objects. Training these networks to deform objects geometrically in images has remained an unresolved challenge. In contrast, P2P-NET is designed to learn geometric transforms between 3D shapes; it requires paired training data, but not paired points.

**Bidirectionality vs. cycle consistency.** Our design of the bidirectional P2P-NET drew inspirations from dual learning [Yi et al. 2017] and the use of cycle consistency loss [Zhu et al. 2017]. What is common about these works is that they all learn transforms between two domains. The cycle consistency loss is a clever way of dealing with the challenge of not having paired training data from the two domains. However, P2P-NET is not built on a cyclic loss. With paired training data for P2P-NET, we can afford to define the two directional geometry losses, without the inverse mappings. At the same time, the bi-directionality between the two transforms is taken advantage of as we define the extra cross regularization loss to enhance the training. Another distinction lies in how the loss functions are defined: the cycle consistency loss measures pixel-to-pixel differences, while our geometry loss measure a *shape-wise* difference between two point sets.

### 3 BIDIRECTIONAL P2P-NET

The architecture of bidirectional P2P-NET is illustrated in Fig. 2. Our training set consists of paired point sets  $\{X, Y\}$  with prior relations among them. The transformations between two sets  $X$  and  $Y$  are latent, hard to explicitly model. For instance,  $X$  can be a single-view point scan of a chair, and  $Y$  contains complete surface samples of the same chair. Another example is depicted in Fig. 3, where a 2D point set sampled from a dog shape is transformed to be a cat.

To realize this bidirectional architecture on unordered point sets, we develop a geometric loss (Section 3.1) that is order-invariant. Since  $X$  and  $Y$  are not in dense correspondences, i.e., point-wise, we need further regularize the loss to balance the mapping and the global distribution of the displacements. To this end, the loss of bidirectional transformations is tightly coupled with a cross regularization (Section 3.2) that maximizes the parallelism between displacements from  $X$ -to- $Y$  and displacements from  $Y$ -to- $X$ .

P2P-NET consists of two network branches from two directions. At each branch, the network first learns a multi-scale feature for each point using layers of PointNet++ [Qi et al. 2017b]. The input point set is down-sampled and point features are constructed in multi-level with set abstraction layers (marked with A in Fig. 2). Then point-wise multi-scale features are produced with the feature propagation layers (marked with P in Fig. 2). The multi-scale point-wise features

are concatenated with the same number of point-wise noise vectors. Each noise vector is an independent Gaussian noise vector of length 32. The feature-noise vectors are fed to a set of fully connected layers that output displacement vectors  $\mathcal{I}_X$ . In the end output layer, the network yields the predicted point set  $\hat{Y} = X + \mathcal{I}_X$ . See Appendix A.1 for a detailed description of the network architecture.

As the network predicts unordered point sets, the loss function only constraints the overall behavior of point sets, while some individual points in a set still have risk in local over-fitting. Our point-wise noises augment the training set in feature vector space by appending random variables to the feature vectors. Added new dimensions of random variables give each point its own variation during training, enabling them to escape from local over-fitting, and meanwhile preserve local smoothness of the predicted point set; compare Figs. 3(a) and 3(b). As the noises introduce stochasticity into the network, we can feed an input point set multiple times during test to obtain a dense output point set; see Fig. 8 for examples.

In addition to the geometric loss defined over the two input and output ends, the aforementioned cross regularization over the transformation displacements strengthens the coupling between two directional networks. The ablation study shown in Fig. 3(c) demonstrates the effectiveness of cross regularization.

#### 3.1 Geometric Losses

To measure the geometric difference between the predicted and target point sets, the network is trained with a loss that consists of two terms. One term penalizes points that do not match with the target shape, and the other term measures the discrepancy of local point density between two corresponding point sets.

The shape matching loss computes the sum of differences between shape of transformed point set  $\hat{Y} = X + \mathcal{I}_X$  and shape of target point set  $Y$ , vice versa between  $\hat{X} = Y + \mathcal{I}_Y$  and  $X$ , by searching the closest point from target point set for each displaced source point:

$$L_{\text{shape}}(\hat{Y}, Y) = \sum_{p \in \hat{Y}} \min_{q \in Y} d(p, q) + \sum_{q \in Y} \min_{p \in \hat{Y}} d(p, q),$$

where  $d(p, q)$  measures  $L_2$  distance between points  $p$  and  $q$ .

This symmetric shape matching term is close to Hausdorff distance between shapes, except that we compute sum of closest distances instead of their maxima. The summation operation makes the loss function differentiable w.r.t. the displaced points, and encourages the displaced point set to match the target tightly.

In addition, we also compute a density loss. For each point  $p$  in target point set  $Y$ , we define local density measures w.r.t.  $Y$  and  $\hat{Y}$ , respectively, using two  $k$ -D vectors ( $k = 8$  by default):

$$\begin{aligned} & [d(p, N_1(Y, p)) \quad d(p, N_2(Y, p)) \quad \dots \quad d(p, N_k(Y, p))], \\ & [d(p, N_1(\hat{Y}, p)) \quad d(p, N_2(\hat{Y}, p)) \quad \dots \quad d(p, N_k(\hat{Y}, p))]. \end{aligned}$$

Here we denote  $N_i(Y, p)$  as the  $i$ -th closest point to  $p$  from the same target point set  $Y$ , and  $N_i(\hat{Y}, p)$  is the  $i$ -th closest point to  $p$  from the predicted point set  $\hat{Y}$ .

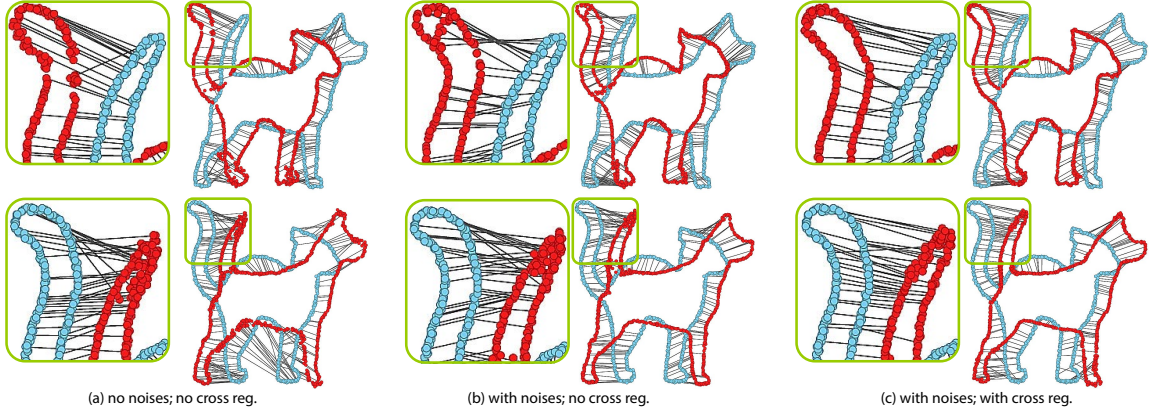


Fig. 3. Ablation study with a toy example (cat & dog). The transformations were learned from a dataset synthesized by randomly rotating and scaling a pair of 2D point sets in the shapes of dog and cat, respectively. The top row shows the transformations from dog (blue) to cat (red), and the bottom row shows from cat (blue) to dog (red). For a clear visualization, we randomly plot only 20% of the displacement vectors using black lines.

These two  $k$ -D vectors encode density measures of  $Y$  and  $\hat{Y}$  in small neighborhoods for each point  $p \in Y$ . The density of predicted point set  $\hat{Y}$  resembles the density of target set  $Y$  if and only if the density vectors of  $\hat{Y}$  are similar to that of  $Y$ . Thus, the density loss is defined as the integration of distances between density vectors of  $\hat{Y}$  and  $Y$  over all points in  $Y$ :

$$L_{\text{density}}(\hat{Y}, Y) = \frac{1}{k} \sum_{p \in Y} \sum_{i=1}^k |d(p, N_i[Y, p]) - d(p, N_i[\hat{Y}, p])|.$$

With a setting of single  $X$ -to- $Y$  transformation network, the geometric loss function is then as follow:

$$L_{X \rightarrow Y}(\mathcal{D}) = \sum_{\{X, Y\} \in \mathcal{D}} \left( L_{\text{shape}}(\hat{Y}, Y) + \lambda L_{\text{density}}(\hat{Y}, Y) \right),$$

and similarly to the other direction:

$$L_{Y \rightarrow X}(\mathcal{D}) = \sum_{\{X, Y\} \in \mathcal{D}} \left( L_{\text{shape}}(\hat{X}, X) + \lambda L_{\text{density}}(\hat{X}, X) \right),$$

where  $\mathcal{D}$  denotes our training set, with a weighting  $\lambda = 1$  by default.

### 3.2 Cross Regularization

We couple the transformations  $X$ -to- $Y$  and  $Y$ -to- $X$  by a cross regularization over their displacement vectors  $\mathcal{I}_X$  and  $\mathcal{I}_Y$ . The key observation is that when  $\mathcal{I}_X$  and  $\mathcal{I}_Y$  are encouraged to be parallel to each other, the two transformations can be mutually enhanced, with a more uniform distribution of the displacement mapping.

The regularization term maximizes the parallelism between  $\mathcal{I}_X$  and  $\mathcal{I}_Y$ , without having paired displacements. For each point  $p \in X$ , or each point  $q \in Y$ , the displacements are associated with 6D vectors  $[p, p + \mathcal{I}_Y(p)]$  or  $[q + \mathcal{I}_X(q), q]$ , respectively. The regularization

works in 6D in a similar manner as computing  $L_{\text{shape}}$ . That is:

$$L_{\text{reg}}(X, Y) = \sum_{p \in X} \min_{q \in Y} d([p, p + \mathcal{I}_Y(p)], [q + \mathcal{I}_X(q), q]) + \sum_{q \in Y} \min_{p \in X} d([p, p + \mathcal{I}_Y(p)], [q + \mathcal{I}_X(q), q]).$$

Minimizing  $L_{\text{reg}}$  in 6D results in maximizing the parallelism between 3D displacement vectors with two opposite directions from bidirectional transformations. See Fig. 3(c) that depicts the enhancement on a 2D toy example by adding cross regularization. More elaborated evaluation is provided in result Section 4.

Given the displacement regularization that couples the transformations  $X$ -to- $Y$  and  $Y$ -to- $X$ , the network is trained with a loss function that sums three terms:

$$L_{X \rightarrow Y}(\mathcal{D}) + L_{Y \rightarrow X}(\mathcal{D}) + \mu \sum_{\{X, Y\} \in \mathcal{D}} L_{\text{reg}}(X, Y), \quad (1)$$

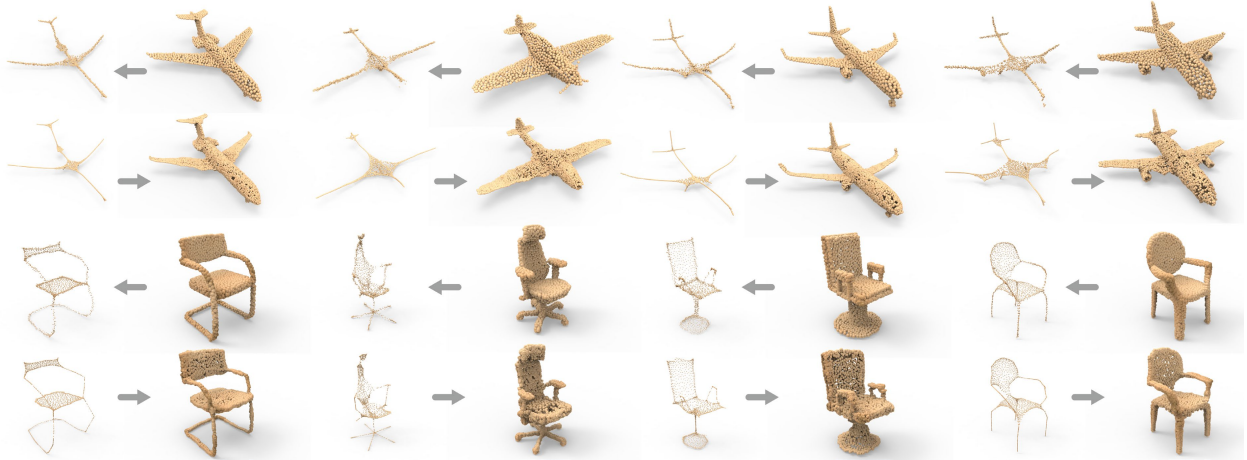
with a balancing parameter  $\mu$  set as 0.1 by default.

We minimize the loss (1) with an Adam optimizer. The learning rate is set as  $1e-3$  and decays to  $1e-4$  at discrete intervals during training.

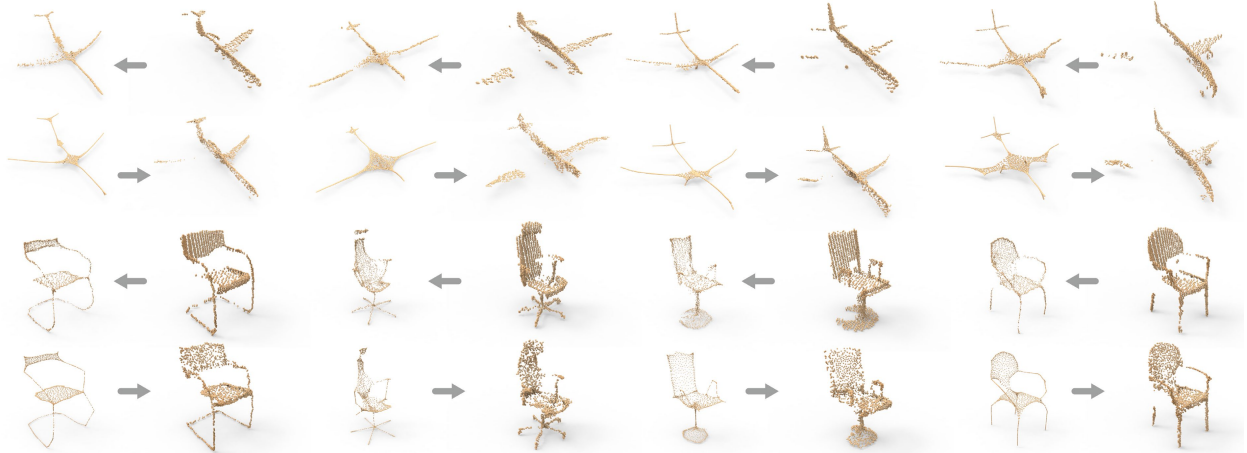
## 4 EXPERIMENTAL RESULTS AND APPLICATIONS

We conduct experiments to demonstrate the capability of P2P-NET in learning geometric transforms between point sets in various domains. Throughout the experiments, the network was trained using different datasets and for different domain pairs separately, but always with the same default network settings as described in Section 3 and Appendix A.1. There is no hyperparameter or architecture tuning for any specific domains or any specific datasets. All the results are presented without any post-processing.

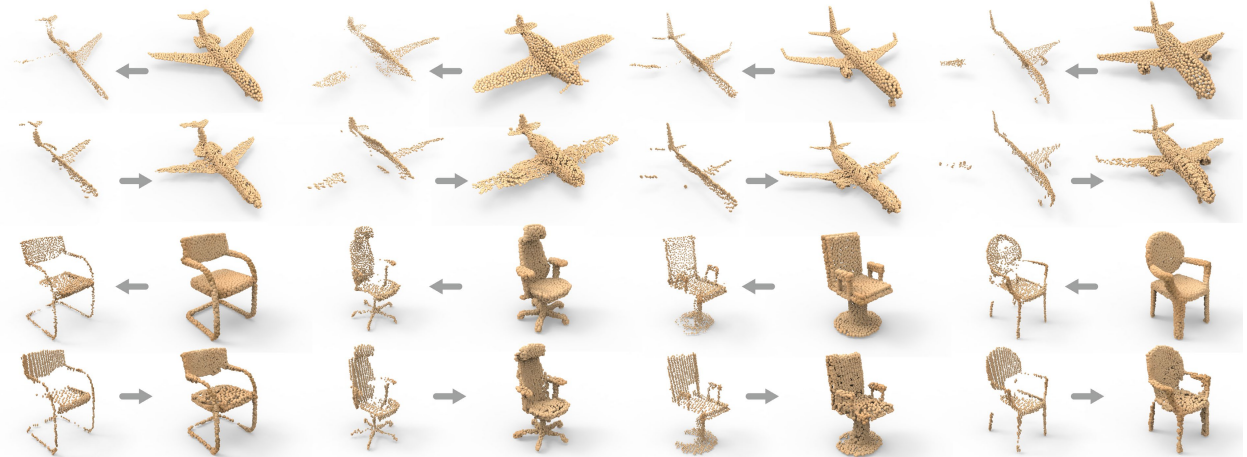




(a) Transformations between meso-skeleton and surface samples. The 2nd and 4th rows show transformations from meso-skeleton (left) to surface samples (right). The 1st and 3rd rows show transformations from surface samples (right) to meso-skeleton (left).



(b) Transformations between meso-skeleton and point scan. The 2nd and 4th rows show transformations from meso-skeleton (left) to point scan (right). The 1st and 3rd rows show transformations from point scan (right) to meso-skeleton (left).



(c) Transformations between point scan and surface samples. The 2nd and 4th rows show transformations from point scan (left) to surface samples (right). The 1st and 3rd rows show transformations from surface samples (right) to point scan (left).

Fig. 4. A gallery of point set transformations among meso-skeletons, shape surfaces, and single-view point scans via our network P2P-NET. Note that, to obtain the transformed surface point samples, we feed the same input eight times to the network and integrate the network outputs to produce a dense point set.

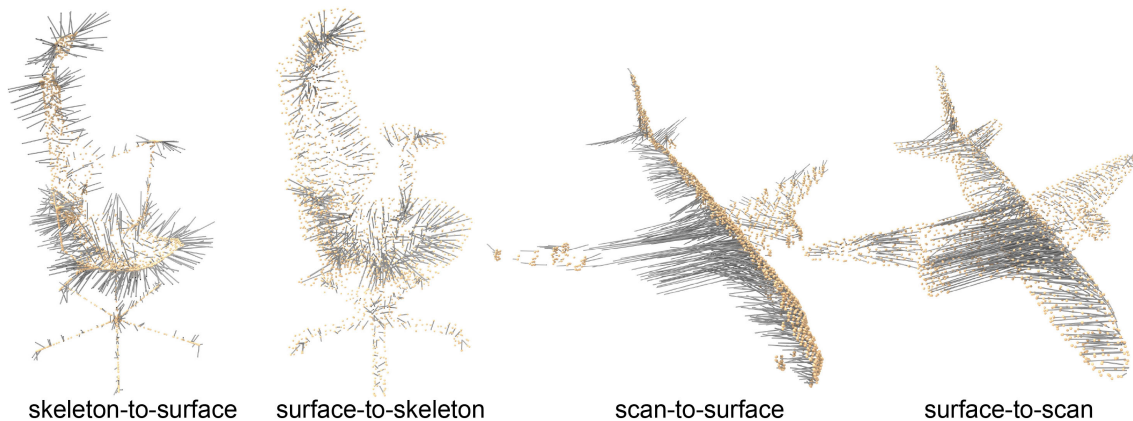


Fig. 5. Visualization of vectors (grey lines) depicting point-wise displacements learned by P2P-NET for various domain mappings, where the source point sets are rendered in orange. Note that for ease of visualization, only 30% of the vectors are displayed and we do not show the target point sets.

#### 4.1 Meso-skeleton, surface, and single-view point scan

In many cases, a mapping from one domain to another is easy, but the inverse is a lot more difficult. For example, synthesizing point scans from 3D shapes is easy, but surface completion is hard. Skeleton extraction from 3D shapes may have been considered as a solved problem [Tagliasacchi et al. 2016], but synthesizing shape surfaces from skeletons is an unresolved challenge. Our network is able to learn to solve ill-posed inverse mapping problems (e.g., skeleton-to-surface) by using training data synthesized by an algorithm designed for the easier transform (e.g., surface-to-skeleton). In this section, we demonstrate transformations among meso-skeletons, surface samples, and single-view point scans using P2P-NET.

Given a set of 3D shapes, we convert them to surface samples with Poisson disk sampling [Corsini et al. 2012]. By taking the surface samples as input, meso-skeletons of the shapes are obtained using a contraction-based approach [Cao et al. 2010]. To show the robustness of our network to shape occlusion, we also synthesize single view point scans with a Kinect simulator [Bohg et al. 2014; Gschwandtner et al. 2011] applied to 3D shapes. We use the chair and airplane datasets of ModelNet40 [Wu et al. 2015b] as original 3D shapes, and sample each point set to the size of 2,048. The chair dataset contains 889 training and 100 test examples. Similarly, the airplane dataset contains 626 training and 100 test examples.

With the synthesized surface samples, meso-skeletons, and single-view point scans, we tested our method on three pairs of transformations among the three different types of point sets, i.e., meso-skeleton vs. surface, meso-skeleton vs. point scan, and point scan vs. surface. In Figure 4, visual results of the three pairs of transformations are provided with eight distinctive examples chosen from the test set. Note that, to obtain transformed surface point samples, we feed the same input in eight passes to P2P-NET and integrate the network outputs to produce a dense final result. To obtain point scans or meso-skeletons, we only feed the input once to the network. Note also that our method does not assume that the input point clouds have uniform density.



Fig. 6. Testing P2P-NET on real chair scans (middle) captured by Kinect v2. The completed point cloud is shown on the right.

To convey that our network is able to learn a shape transform, we show the closest training examples retrieved for the inputs over the eight test examples in Appendix A.2. We also provide quantitative evaluation for the three pairs of transformations in Section 4.3.

Figure 5 visualizes point-wise displacements produced by P2P-NET to offer a glimpse of what the network learned. We re-emphasize that the network was not trained on any point-wise mapping between paired shapes nor with any displacement vectors. Yet, it appears that the learned displacements are well localized and reflect what a properly devised transformation algorithm would produce.

In Figure 6, we show that the trained P2P-NET is capable of converting real point scans of chairs captured by a Kinect v2 to complete shapes. Note that during the capture, the Kinect sensor was placed to roughly align with the camera view used in data synthesis.

The results shown in Figure 4 demonstrate the potential of P2P-NET for possible applications. In Figure 7, we show such an example for shape editing and synthesis. After combining the meso-skeletons of different shapes into a new meso-skeleton, our network can convert



Fig. 7. After editing and combining the point sets of meso-skeletons, our network is able to generate new shapes (right) from the new meso-skeletons.

the synthesized meso-skeleton into a new point-set shape. Moreover, the result of transforming point scans to surface samples offers promises of applying P2P-NET for scan completion. To extend P2P-NET to a full-fledged scan completion network, one would require a multi-view assembly of the network or adding a view prediction and rotation layer, which are out of the scope of this paper.

#### 4.2 2D cross-sectional profiles and 3D shapes

Planar cross-sectional profiles are widely used in computer-aided design and geometric modeling. Transforming from 2D cross sections to 3D shapes is an interesting test for our neural network. For this experiment, we use the sofa and bed datasets of ModelNet40. The sofa dataset contains 680 training and 100 test examples. Similarly, in the bed dataset, there are 515 training and 100 test examples. We cut each sofa with four parallel planes to obtain four parallel cross sections, and cut each bed with three orthogonal planes to obtain three orthogonal cross sections. We sample each set of cross sections uniformly to acquire a point set consisting of 2,048 points. Each point set of cross sections is then paired with the point set of mesh samples of the same sofa or bed object.

We visualize results obtained on eight typical test examples of sofa and bed in Figure 8. We can observe that the transformation results obtained with feeding the network a single input pass exhibit non-uniformity and missing regions. However, after feeding the input over eight passes and integrating the network outputs, the resulting dense point sets are complete and smooth overall. This demonstrates the stability of transformation prediction by P2P-NET.

It is also interesting to observe that in some cases, the dense outputs produced by multiple passes of P2P-NET can better convey shape details than the ground truth data, e.g., see column (c) in Figure 8 for the long pillow in the fifth row and the slats in the crib in the second to last row, in contrast to their counterparts in column (d). One reason is that the ground truth is only at  $1/8$  of the resolution compared to the dense results. On the other hand, the level of surface details produced by the network are not copied from the training set

since all training data are at a low resolution of 2,048 points which do not well reflect the surface details. The produced details should be attributed to the point transforms learned by P2P-NET.

To further demonstrate that the network has learned a proper transform, we retrieved the closest training cross sections with the test cross sections as query inputs, and show the retrieved cross sections and their paired sampled meshes in Figure 8. The retrieval was carried out using the distance measure:

$$D_{\text{retrieve}}(P, Q) = \sum_{p \in P} \min_{q \in Q} \|p - q\| + \sum_{q \in Q} \min_{p \in P} \|p - q\|,$$

where  $P$  and  $Q$  are two point sets of cross sections.

We can observe that the retrieved cross sections are generally not close to the queries; this is clearly evident in the last three rows of Figure 8. Admittedly, it is far from trivial to come up with an accurate similarity distance measure for cross-sectional profiles. To confirm that the retrieved results are reasonable, we have manually examined all the training examples in the dataset and found no other cross sections to be visually closer to those shown in the figure.

In Figure 9, we visualize the displacement vectors learned for the current transform. Since mappings from cross-sectional profiles to 3D shapes are a lot less predictable and coherent, instead of showing the displacement vectors explicitly like in Figure 5, we show a morphing sequence following the displacements.

What is common between skeleton-to-shape and profile-to-shape transforms is that one domain has an *easy-to-edit* shape abstraction. It is quite common to perform user edits on skeletons and curve profiles. It would certainly be desirable then, to be able to directly convert the edited shape abstractions to whole shapes. Like the example shown in Figure 7, we also experimented with editing 2D cross-sections and then transforming the edits to 3D point-set shapes using P2P-NET. A visual result showing an interpolating sequence is provided in Figure 1, further demonstrating the potential of our network in shape synthesis applications.

#### 4.3 Quantitative evaluation

We evaluated the performance of our P2P-NET quantitatively on the four datasets used in Section 4.1 and 4.2. For the purpose of measuring the errors, the original shapes and their point sets were normalized such that the diagonal lengths of their bounding boxes are equal to 1. We remind that all the training and test point sets are sampled to the size of 2,048. The performances were measured with three error metrics as detailed below.

**Point separation rate.** Given a predicted point set and the ground-truth point set, each point searches for its closest point from the opposite set. If the distance from a point  $p$  to its closest point  $q$  in the opposite set is greater than 0.02, we consider the point  $p$  as a separated point. We call the percentage of separated points among all points in the two sets as separation rate. We compute separation rate for every test example and report the mean in Table 1.



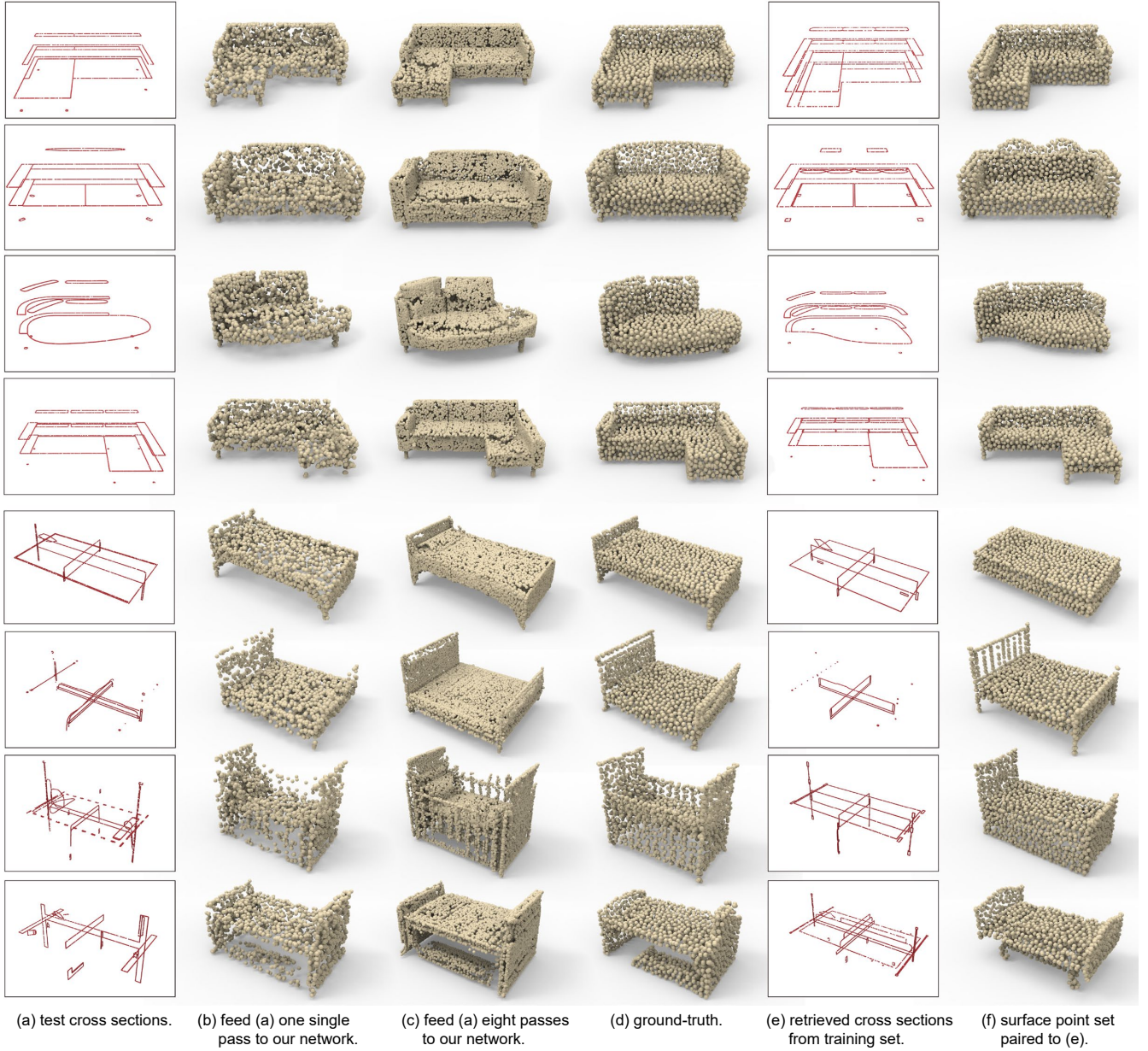


Fig. 8. Transformations from 2D cross-sectional profiles (a) to 3D object surfaces (b) and (c). In addition to ground-truths (d), we also provide the closest 2D cross-sectional profiles (e) retrieved from the training set, and their corresponding surface point sets (f).

**Curvature difference.** We estimate a curvature indicator for each point  $p$  as  $\lambda_0/(\lambda_0 + \lambda_1 + \lambda_2)$ , where  $\lambda_0 \leq \lambda_1 \leq \lambda_2$  are the eigenvalues of a  $3 \times 3$  covariance matrix of a local point patch around point  $p$ . The size of the local patch is 0.3% of the size of whole point set. For each point  $p$ , we compute the absolute difference of curvature indicator with its closest point  $q$  in the opposite point set. Finally, we compute the mean difference of all points.

**Normal difference.** Similar to the curvature indicator, we estimate a PCA normal for each point, and measure the radian of the angle

between the normal of a point  $p$  and the normal of its closest point  $q$  in the opposite set. We compute the mean radian of all points.

For each pair of transformations on each dataset, we trained the networks for 200 epoches on a Nvidia Titan Xp GPU that takes approximately 5~8 hours to finish the process. During the testing phase, when the target point set is not from surface samples, we feed the source point set in one single pass to the network and obtain output point sets of size 2,048. When the target point set is from surface samples, we feed the source point set in eight passes to the network

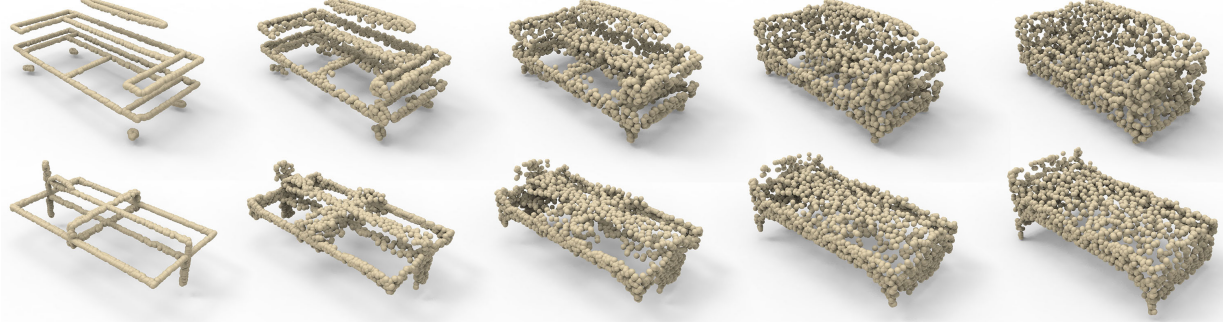


Fig. 9. Visualization of point displacements learned by P2P-NET which transform cross-sectional profiles into surface samples. We scaled the displacements, from left to right, by factors of 0.05, 0.25, 0.5, 0.75, 1.0, respectively, to obtain a morphing sequence.

Dataset	Source	Target	mean of separation rate			mean of curvature diff.			mean of normal diff.		
			ns-rg-	ns+rg-	ns+rg+	ns-rg-	ns+rg-	ns+rg+	ns-rg-	ns+rg-	ns+rg+
airplane	skeleton	surface	1.4%	<b>0.6%</b>	<b>0.6%</b>	0.084	0.063	<b>0.062</b>	0.575	0.390	<b>0.389</b>
	surface	skeleton	<b>0.3%</b>	0.4%	<b>0.3%</b>	0.076	0.076	<b>0.075</b>	-	-	-
	scan	skeleton	2.1%	<b>2.0%</b>	<b>2.0%</b>	0.068	0.068	<b>0.066</b>	-	-	-
	skeleton	scan	2.9%	<b>2.3%</b>	2.4%	<b>0.051</b>	0.052	0.052	0.677	0.617	<b>0.601</b>
	scan	surface	1.6%	<b>1.2%</b>	1.3%	0.074	0.063	<b>0.061</b>	0.495	0.444	<b>0.418</b>
	surface	scan	1.3%	<b>1.1%</b>	1.3%	<b>0.056</b>	0.057	0.057	0.669	0.670	<b>0.667</b>
chair	skeleton	surface	12.0%	<b>7.5%</b>	<b>7.5%</b>	0.096	0.082	<b>0.080</b>	0.686	0.620	<b>0.617</b>
	surface	skeleton	5.3%	5.3%	5.3%	0.061	0.061	<b>0.060</b>	-	-	-
	scan	skeleton	15.5%	15.8%	<b>15.4%</b>	0.053	0.053	<b>0.051</b>	-	-	-
	skeleton	scan	18.8%	17.6%	<b>17.5%</b>	<b>0.052</b>	0.054	<b>0.052</b>	0.590	0.584	<b>0.562</b>
	scan	surface	10.9%	<b>6.6%</b>	6.7%	0.092	<b>0.083</b>	0.084	0.613	0.557	<b>0.553</b>
	surface	scan	5.2%	5.2%	<b>4.9%</b>	0.057	0.057	<b>0.056</b>	0.553	0.556	<b>0.552</b>
sofa	cross sec.	surface	22.0%	<b>9.8%</b>	10.8%	0.084	0.066	<b>0.065</b>	0.626	<b>0.457</b>	0.458
	surface	cross sec.	9.6%	9.2%	<b>8.9%</b>	<b>0.059</b>	0.060	<b>0.059</b>	-	-	-
bed	cross sec.	surface	14.5%	3.0%	<b>2.9%</b>	0.084	<b>0.056</b>	<b>0.056</b>	0.544	<b>0.380</b>	<b>0.380</b>
	surface	cross sec.	<b>11.0%</b>	11.8%	11.5%	0.058	0.058	0.058	-	-	-

Table 1. Quantitative evaluation of our network with different settings and error metrics. In the head of table, ‘ns’ stands for noise augmentation, ‘rg’ stands for cross regularization, and ‘+/-’ indicates enable/disable.

to obtain an integrated dense output of size 16,384. Four pairs of transformations and three different settings of the network were tested and reported in Table 1. The three different settings of network include, no noise augmentation and no cross regularization(ns-rg-), no noise augmentation but with cross regularization(ns-rg+), with noise augmentation and with cross regularization(ns+rg+).

Note that the separation rate measures tightness of the match between predicted point set and ground-truth point set. The smaller the value is, the tighter the match. The results in Table 1 show that noise augmentation helps to reduce the separation rate, i.e., to make the predicted points to match more tightly to the ground-truth point sets. Adding the cross-regularization does not further reduce the separation rate. However, as shown in Table 1, adding the cross-regularization term does achieve lower error rates overall in terms of curvature difference and normal difference. Since these two measures reflect how well local geometric properties of the point set are preserved, the quantitative results demonstrate that

cross-regularization is effective in enhancing the local geometric properties of the predicted point set.

## 5 DISCUSSION, LIMITATION, AND FUTURE WORK

By design, P2P-NET is a general-purpose point-to-point displacement network, in that no parts of the network is tailor-made to purposely target specific transformation tasks. Moreover, we do not alter the network architecture when dealing with different pairs of transformation domains. The network is trained to map point sets from one domain to another, where the point sets can be in 2D or 3D spaces. As we demonstrated, the mapping can also lift 2D profiles to 3D shapes; see Figure 8. Indeed, since the mapping is applied in a feature space, the learned transform is agnostic to the dimensionality of the point sets. Interestingly, the point displacements, which are one-to-one, are learned without training data on point-wise mapping nor displacement vectors. All we provide are pairs of point-set shapes, which may even have different cardinalities.

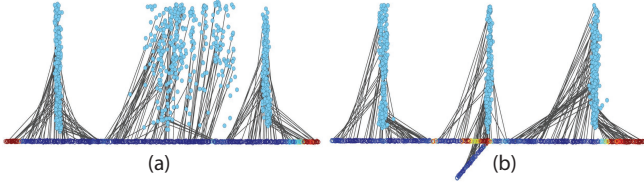


Fig. 10. P2P-NET cannot be properly trained to map a horizontal line to three vertical bars since points near the mid-section possess similar point features. Our method fails to associate points with similar features with dissimilar displacements to clearly form the middle bar (a). However, a small added protrusion (b) can serve to disambiguate these point features, leading to different displacements to produce the middle bar. Colorings of the points reflect their features, after a 1D embedding using PCA.

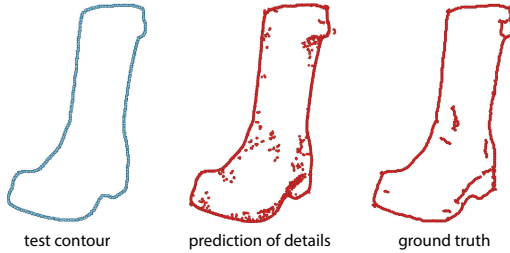


Fig. 11. P2P-NET cannot be properly trained for non-deterministic point set transforms, e.g., adding details to a shape contour.

P2P-NET is bidirectional, which may be reminiscent of networks trained under cycle consistency [Yi et al. 2017; Zhu et al. 2017]. However, there is no cyclic consistency in P2P-NET; the bidirectionality is used to form a cross-regularization that exploits the two mappings to enhance the mapping distribution. There is an intriguing, and seemingly “dual”, relation between P2P-NET and CycleGAN [Zhu et al. 2017]. P2P-NET is trained on paired shapes, while CycleGAN learns from unpaired images. But in CycleGAN, there is pixel-to-pixel correspondence between the pair of training images; P2P-NET does not require point-to-point correspondence between the training point-sets. CycleGAN is trained to learn how to transform pixel values, *in place*, while Point-NET is trained to displace points from one shape representation to another.

We reiterate that our work is only a first attempt at designing a general-purpose shape transformation network. By no means should one expect P2P-NET to work effectively for all transformation tasks. The network is inherently limited by its current architecture, training loss, and optimization scheme for the network parameters. In what follows, we provide a non-exhaustive list of such limitations to explore the behavior and limit of our method.

**Ambiguous feature-to-displacement mapping.** In the absence of point-to-point correspondences between the training source and target shapes, P2P-NET must learn point set transforms implicitly. Architecturally, P2P-NET first turns the input points into PointNET++ features. It then learns to map these point features to displacement vectors to minimize the training loss. As a result, P2P-NET should be trained with examples where the implicit relation

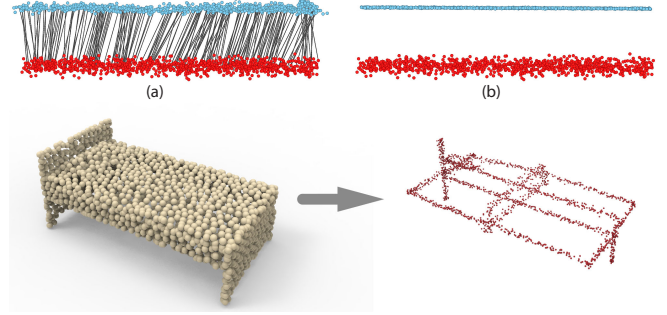


Fig. 12. P2P-NET cannot be trained to accurately and cleanly predict thin structures. Top: from a noisy input (red), as shown in (a), in contrast to the ground truth (b). Bottom: from lower-resolution point set inputs.

between point features and displacements is *unambiguous*. The network should not be expected to learn to associate points possessing similar features with *different* displacements. In reality however, ambiguous feature-to-displacement mappings may be unavoidable for many transformation tasks. Moreover, they may be characteristic of an entire class of transformations or occur only for some shape pairs or only over a portion of the shapes. Any such case may potentially lead to failure cases by P2P-NET.

To provide a simple illustration, consider a 2D example of learning to map points along a horizontal line to three vertical bars, as shown in Figure 10. We trained P2P-NET using more than 1,000 examples of source and target pairs in random orientations and scales. However, regardless of how many training examples we employed, the network still cannot map the mid-section of the line to the middle bar since points near the mid-section all possess similar features. As shown in (a), P2P-NET could only learn to associate these points with similar displacements. To verify that the crux of the problem is the ambiguity, we added a small protrusion under the source line so that points near the mid-section can be better distinguished by PointNET++ features. As can be seen in (b), now P2P-NET does a much better job of learning the proper transform.

**Ambiguous point transforms.** Some point set transforms may exhibit shape-level ambiguities, as shown in Figure 11. The task is to learn displacements from a shape silhouette to its interior details. The training set contains more than 1,000 examples of adding details (via edge maps) to the *same* boot shape. To minimize the training loss, P2P-NET is only able to learn to displace to an *average* of the target points, leading to an erroneous outcome.

**Decorrelation of displacements.** The training loss adopted by P2P-NET is predominantly a point-to-shape distance measure; it does not account for intrinsic properties of the input shape. This immediately implies that P2P-NET would not learn such properties to possibly preserve them in the output point clouds. The point displacement vectors predicted by P2P-NET are not correlated or controlled by the shape properties as the network predicts a displacement vector for each point independently. Figure 12 shows that P2P-NET is unlikely to reproduce thin lines when all the training



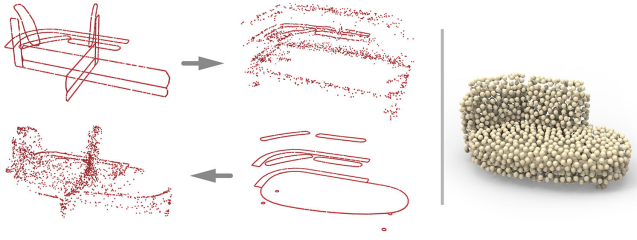


Fig. 13. P2P-NET cannot be trained to produce highly structured point sets cleanly, e.g., to transform between orthogonal profiles and parallel profiles for the same 3D shape (sofa on the right).

data contain clean, thin line structures. Figure 13 shows that P2P-NET cannot be well trained to produce highly structured point sets, where the transform is between orthogonal profiles and parallel profiles of the same shapes. By the same token, P2P-NET is not part-aware, i.e., it is unlikely to preserve part structures of the input shapes. For examples, it cannot transform clean rooms into messy rooms, by displacing or adding point-set objects; only uncorrelated point-wise displacements are currently learned.

**Future work.** In addition to address the limitations discussed so far, a network capable of transforming point sets *hierarchically* is likely to produce more fine-grained results and adapt to more domains. We would also like to consider *transitive* transformations, where a source shape reaches a target via a sequence of two networks through an intermediate shape. On that shape, the points can be upsampled, consolidated, filtered or undergoing any other processing operation. This may also be generalized to combining and composing transformations. Finally, an intriguing avenue for future research would be to relax the need for paired shapes, and replace it with an unsupervised or weakly supervised setting to train a general-purpose network for point set transforms.

## REFERENCES

- Marc Alexa, Johannes Behr, Daniel Cohen-Or, Shachar Fleishman, David Levin, and Claudio T. Silva. 2003. Computing and rendering point set surfaces. *IEEE Trans. Vis. & Comp. Graphics* 9, 1 (2003), 3–15.
- Matthew Berger, Andrea Tagliasacchi, Lee M. Seversky, Pierre Alliez, Gaël Guennebaud, Joshua A. Levine, Andrei Sharf, and Claudio T. Silva. 2017. A Survey of Surface Reconstruction from Point Clouds. *Computer Graphics Forum* 36, 1 (2017), 301–329.
- Sema Berkiten, Maciej Halber, Justin Solomon, Chongyang Ma, Hao Li, and Szymon Rusinkiewicz. 2017. Learning detail transfer based on geometric features. In *Computer Graphics Forum (Eurographics)*, Vol. 36. 361–373.
- Jeannette Bohg, Javier Romero, Alexander Herzog, and Stefan Schaal. 2014. Robot arm pose estimation through pixel-wise part classification. In *Proc. of ICRA*. IEEE, 3143–3150. [https://github.com/jbohger/render\\_kinect](https://github.com/jbohger/render_kinect)
- Arunkumar Byravan and Dieter Fox. 2016. SE3-Nets: Learning Rigid Body Motion using Deep Neural Networks. (2016).
- Junjie Cao, Andrea Tagliasacchi, Matt Olson, Hao Zhang, and Zhixun Su. 2010. Point cloud skeletons via laplacian based contraction. In *Proc. IEEE Int. Conf. on Shape Modeling and Applications*. 187–197.
- Jonathan C Carr, Richard K Beatson, Jon B Cherrie, Tim J Mitchell, W Richard Fright, Bruce C McCallum, and Tim R Evans. 2001. Reconstruction and representation of 3D objects with radial basis functions. In *ACM Trans. on Graph (SIGGRAPH)*. 67–76.
- Massimiliano Corsini, Paolo Cignoni, and Roberto Scopigno. 2012. Efficient and flexible sampling with blue noise properties of triangular meshes. *IEEE Trans. Vis. & Comp. Graphics* 18, 6 (2012), 914–924.
- Angela Dai, Charles Ruizhongtai Qi, and Matthias Nießner. 2017. Shape Completion using 3D-Encoder-Predictor CNNs and Shape Synthesis. In *Proc. of CVPR*.
- Haoqiang Fan, Hao Su, and Leonidas Guibas. 2017. A point set generation network for 3d object reconstruction from a single image. In *Proc. of CVPR*.
- Matheus Gadelha, Subhransu Maji, and Rui Wang. 2017. Shape Generation using Spatially Partitioned Point Clouds. In *Proc. of BMVC*.
- Markus Gross and Hanspeter Pfister. 2007. *Point-Based Graphics*. Morgan Kaufmann.
- Michael Gschwandtner, Roland Kwitt, Andreas Uhl, and Wolfgang Pree. 2011. BlenSor: blender sensor simulation toolbox. *Advances in visual computing* (2011), 199–208.
- Paul Guerrero, Yanir Kleiman, Maks Ovsjanikov, and Niloy J Mitra. 2017. PCP-NET: Learning Local Shape Properties from Raw Point Clouds. *arXiv preprint arXiv:1710.04954* (2017).
- Ruizhen Hu, Wenchao Li, Oliver van Kaick, Hui Huang, Melinos Averkiou, Daniel Cohen-Or, and Hao Zhang. 2017. Co-Locating Style-Defining Elements on 3D Shapes. *ACM Trans. on Graph* 36, 3 (2017), 33:1–33:15.
- Hui Huang, Dan Li, Hao Zhang, Uri Ascher, and Daniel Cohen-Or. 2009. Consolidation of unorganized point clouds for surface reconstruction. In *ACM Trans. on Graph (SIGGRAPH Asia)*, Vol. 28. 176:1–176:7.
- Hui Huang, Shihao Wu, Daniel Cohen-Or, Minglun Gong, Hao Zhang, Guiqing Li, and Baoquan Chen. 2013a. L1-medial skeleton of point cloud. *ACM Trans. on Graph (SIGGRAPH)* 32, 4 (2013), 65:1–65:8.
- Hui Huang, Shihao Wu, Minglun Gong, Daniel Cohen-Or, Uri Ascher, and Hao Zhang. 2013b. Edge-aware point set resampling. *ACM Trans. on Graph* 32, 1 (2013), 9:1–9:12.
- Hui Huang, Shihao Wu, Minglun Gong, Daniel Cohen-Or, Uri Ascher, and Hao Zhang. 2013c. Edge-aware Point Set Resampling. *ACM Trans. on Graph* 32, 1 (2013), 9:1–9:12.
- Phillip Isola, Jun-Yan Zhu, Tinghui Zhou, and Alexei A Efros. 2017. Image-to-image translation with conditional adversarial networks. In *Proc. of CVPR*.
- Max Jaderberg, Karen Simonyan, Andrew Zisserman, et al. 2015. Spatial transformer networks. In *Proc. of NIPS*. 2017–2025.
- Michael Kazhdan and Hugues Hoppe. 2013. Screened Poisson surface reconstruction. *ACM Trans. on Graph* 32, 3 (2013), 29:1–29:13.
- Chen-Hsuan Lin, Chen Kong, and Simon Lucey. 2018. Learning Efficient Point Cloud Generation for Dense 3D Object Reconstruction. In *Proc. of AAAI*.
- Yaron Lipman, Daniel Cohen-Or, David Levin, and Hillel Tal-Ezer. 2007. Parameterization-free projection for geometry reconstruction. In *ACM Trans. on Graph (SIGGRAPH)*, Vol. 26. 22:1–22:6.
- Ming-Yu Liu, Thomas Breuel, and Jan Kautz. 2017. Unsupervised Image-to-Image Translation Networks. In *Proc. of NIPS*. 700–708.
- Zhaoliang Lun, Matheus Gadelha, Evangelos Kalogerakis, Subhransu Maji, and Rui Wang. 2017. 3D Shape Reconstruction from Sketches via Multi-view Convolutional Networks. In *Proc. of 3DV*.
- Niloy J Mitra and An Nguyen. 2003. Estimating surface normals in noisy point cloud data. In *Symp. on Geom. Proc.* 322–328.
- Matthias Müller, Richard Keiser, Andrew Nealen, Mark Pauly, Markus Gross, and Marc Alexa. 2004. Point based animation of elastic, plastic and melting objects. In *Symp. on Computer Animation*. 141–151.
- Mark Pauly, Richard Keiser, Leif P Kobbelt, and Markus Gross. 2003. Shape modeling with point-sampled geometry. *ACM Trans. on Graph (SIGGRAPH)* 22, 3 (2003), 641–650.
- Reinhold Preiner, Oliver Mattausch, Murat Arikan, Renato Pajarola, and Michael Wimmer. 2014. Continuous Projection for Fast L1 Reconstruction. *ACM Trans. on Graph* 33, 4 (July 2014), 47:1–47:13.
- Charles R. Qi, Hao Su, Kaichun Mo, and Leonidas J. Guibas. 2017a. PointNet: Deep Learning on Point Sets for 3D Classification and Segmentation. In *Proc. of CVPR*.
- Charles R. Qi, Li Yi, Hao Su, and Leonidas J. Guibas. 2017b. PointNet++: Deep Hierarchical Feature Learning on Point Sets in a Metric Space. In *Proc. of NIPS*.
- Minhyuk Sung, Hao Su, Vladimir G Kim, Siddhartha Chaudhuri, and Leonidas Guibas. 2017. ComplementMe: Weakly-Supervised Component Suggestions for 3D Modeling. *ACM Trans. on Graph (SIGGRAPH Asia)* 36, 6 (2017), 226:1–226:12.
- Andrea Tagliasacchi, Thomas Delame, Michela Spagnuolo, Nina Amenta, and Alexandru Telea. 2016. 3D Skeletons. In *Eurographics State of the Art Report*.
- Andrea Tagliasacchi, Hao Zhang, and Daniel Cohen-Or. 2009. Curve skeleton extraction from incomplete point cloud. In *ACM Trans. on Graph (SIGGRAPH Asia)*, Vol. 28. 71:1–71:9.
- Shihao Wu, Hui Huang, Minglun Gong, Matthias Zwicker, and Daniel Cohen-Or. 2015a. Deep Points Consolidation. *ACM Trans. on Graph* 34, 6 (2015), 176:1–176:13.
- Zhirong Wu, Shuran Song, Aditya Khosla, Fisher Yu, Linguang Zhang, Xiaoou Tang, and Jianxiong Xiao. 2015b. 3d shapenets: A deep representation for volumetric shapes. In *Proc. of CVPR*. 1912–1920.
- Zili Yi, Hao Zhang, Ping Tan, and Minglun Gong. 2017. DualGAN: Unsupervised Dual Learning for Image-to-Image Translation. In *Proc. of ICCV*.
- Tinghui Zhou, Shubham Tulsiani, Weilun Sun, Jitendra Malik, and Alexei A Efros. 2016. View synthesis by appearance flow. In *Proc. Euro. Conf. on Comp. Vis.* 286–301.
- Jun-Yan Zhu, Taesung Park, Phillip Isola, and Alexei A Efros. 2017. Unpaired image-to-image translation using cycle-consistent adversarial networks. In *Proc. of ICCV*.



## A APPENDIX

### A.1 Details of network architecture

In this appendix, we provide details of the set abstraction layers, feature propagation layers, and fully connected layers in P2P-NET. We use same notations as in [Qi et al. 2017b]. A set abstraction layer of PointNet++ is denoted as  $SA(K, r, [l_1, \dots, l_d])$ , where  $K$  is number of local patches,  $r$  is radius of balls that bound the patches,  $[l_1, \dots, l_d]$  are widths of fully connected layers used in local PoinNet. A feature propagation layer is denoted as  $FP([l_1, \dots, l_d])$ , where  $[l_1, \dots, l_d]$  are widths of fully connected layers used inside the layer. A fully connected layer is denoted as  $FC(l)$ , where  $l$  is its width. Note that we disabled dropout for the FC layers.

For all experiments shown in the paper, we used same A-P layers:

```
input → SA(1024, 0.1, [64, 64, 128]) → SA(384, 0.2, [128, 128, 256])
→ SA(128, 0.4, [256, 256, 512]) → SA(1, 1.0, [512, 512, 1024])
→ FP([512, 512]) → FP([512, 256]) → FP([256, 128])
→ FP([128, 128, 128]) → feature
```

We also used same fully connected layers:

```
[feature, noise] → FC(128) → FC(64) → FC(3) → displacements
```

### A.2 Closest training examples

In Figs. 14 and 15, we showed the closest models from training set that are retrieved for the test examples used in Section 4.1. The retrieval was done by searching for a training example that has the closest surface samples to an input test example. To measure the difference between surface samples, we use the distance measure  $D_{\text{retrieve}}(P, Q)$  as described in Section 4.2.



Fig. 14. Closest training examples for the test airplanes in Fig. 4.



Fig. 15. Closest training examples for the test chairs in Fig. 4.